Out-of-Plane Permalloy Magnetic Actuators for Delta-Wing Control

Chang Liu, Tom Tsao, Yu-Chong Tai
Electrical Engineering 116-81, California Institute of Technology, Pasadena, CA 91125

Tzong-Shyng Leu, Chih-Ming Ho, Wei-Long Tang, Denny Miu
MANE, The Univeristy of California, Los Angeles, CA 90024

INTRODUCTION

The goal of this project is to demonstrate that a collection of micro-machined actuators can control a macro object, provided that a proper controlling mechanism exists. In our case, we intend to use a linear array of out-of-plane magnetic actuators to create a rolling moment on a tail-less delta-wing model, utilizing a known mechanism in delta-wing theory that allows micro actuation to have an amplified, macro effect.

A delta-wing is one of the fundamental configurations for generating lift forces and its aerodynamic control is of great importance to the aeronautics society [1,2]. When laminar air flow hits the two leading edges of the wing at a certain angle-of-attack (30° in our case, Fig. 1a,b), two counter-rotating leading-edge vortices are separated from the laminar flow and propagate over the wing's top (Fig. 1c). These two high-momentum, low-pressure vortices contribute identical vortex lifting forces on the two sides of the wing, the sum of these being ~40 % of the total lifting forces. The strength and position of these two vortices are determined by the boundary layer conditions near their separation points. A boundary layer is roughly 1-2 mm thick at a wind-tunnel flow speed of less than 20 m/s; the thickness will decrease when the flow speed is increased. Two linear arrays of surface micro-machined out-of-plane actuators (micro-flaps) are placed along two leading edges at the bottom of the wing (Fig. 1d). When un-deflected, flap arrays remain at the bottom of the boundary layer, having no effect on the flow and vortices; when one array is deflected downward, however, it interacts with the boundary layer and changes the separation point of the corresponding leading-edge vortex. The span-wise vortex structures over the top of the wing become unbalanced, and an overall rolling moment can be created.

The delta-wing has a 38-cm span and a 67 ° top angle; it is tested in a wind-tunnel with a top speed of 20 m/s. Silicon micro-machined actuators are chosen here because of their added advantages of light weight and potentially large bandwidth. To control this wing, micro-flaps are required to deflect 1-2 mm out-of-plane (or to match the boundary-layer thickness), and withstand large aerodynamic loading on the order of several hundred μN.

Magnetic actuation is used because it is known to generate stronger and longer-range forces [3, 4, 5] compared with most other driving methods. Several types of magnetic micro-actuators have been previously demonstrated, but none can readily fulfill the current system requirements. Beneck et. al. [6] performed post-processing manual attachments of permanent magnet pieces on micromachined plates and actuated the magnet with an external magnetic field generated by in-plane coils. The manual assembly is unsuitable for us because a large number of actuators is required. At Caltech, we have developed an integrated coil-type magnetic flap with an out-of-plane vertical displacement of several hundred μm and magnetic forces of 10's of μN [7] . However, these flaps require a large current (~50 mA) to operate and have considerable heating problems. Judy et. al., on the other hand, demonstrated the in-plane motion of a suspended polysilicon structure with an electroplated permanent-magnetic plate [8]. The plate was driven by an external magnetic field to a large deflection angle (over 180°), under an estimated torque of over 0.185 nNm.

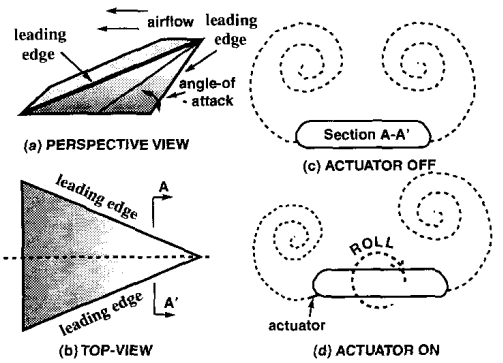

Fig. 1 Fluid mechanisms for delta-wing rolling motion control. (a) Perspective view of a delta-wing in a flow field; (b) top view of the delta-wing; (c) cross-sectional view of the wing and vortex structures when the micro-flaps are off; (d) vortex structures when the micro-flaps along one leading edge are turned on.

The permanent magnet/external magnetic field interaction has so far demonstrated the strongest driving capability and is therefore adopted in our system. Our flap consists of a suspended polysilicon plate with electroplated permalloy over the top; an external magnetic field, perpendicular to the chip substrate, deflects the flap out of plane. In this paper, the design, fabrication and testing of such integrated permalloy micro-flaps are presented.

THEORY

Our actuator consists of a suspended rectangular plate ($L \times W \times t$ in volume) and two parallel supporting beams, with l,w,t being their length, width, and thickness (Fig. 2). The size of the permalloy plate is $L \times W \times T$.

Flow Loading

Fluid-dynamic loading, F_{dl}, can be estimated by [9]

$$F_{dl} = \frac{1}{2}\rho u^2 A, \tag{1}$$

where ρ is the air density ($1.18 kg/m^3$ at 27 °C, [10]), u is the average flow velocity across the flap, and A is the projected area of the flap blocking the flow field. When the entire flap lies within the boundary layer, u is half of the wind-tunnel flow speed.

Static Deflection

The flap's gravitational deflection should be minimized to ensure that it will not drop significantly out-of-plane when the chips are positioned downward. The static deflection, δ, is caused by the weight of the combined polysilicon and permalloy plate; δ_{max} occurs at the free end of the beams. Using the small-deflection assumption [11],

$$\delta_{max} = \frac{Fl^3}{3EI} + \frac{(F\frac{L}{2})l^2}{2EI}, \tag{2}$$

where $F = LW(T \times \rho_{perm} + t \times \rho_{poly})$, $\rho_{perm} \sim 8.9 \times 10^3 kg/m^3$, $\rho_{poly} \sim 2.3 \times 10^3 kg/m^3$, $E = 160 \times 10^9 N/m^2$ is the Young's Modulus of the polysilicon, and $I = (2w)t^3/12$ is the over-all moment of inertia of the two beams.

Magnetic Actuation

Inside a non-uniform magnetic field, magnetic forces can be estimated by a simplified magnetic-charge model, also used in [8]. Assuming that two magnetic charges of opposite polarities are fixed at the two ends of the permalloy plate, and the initial flap position is in favor of the out-of-plane (rather than down-to-the-substrate) motion, two point forces will develop on the two ends of the permalloy plate; their directions are shown in Fig. 3a,b.

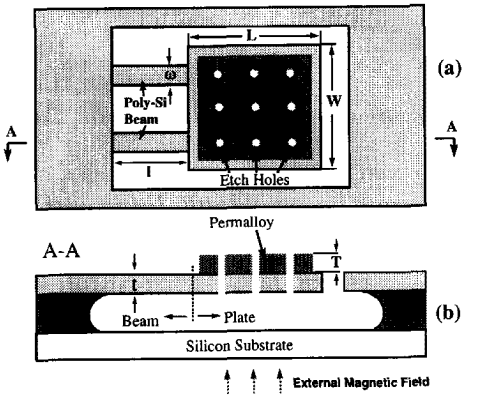

Fig. 2 Schematic of an out-of-plane permalloy magnetic actuator (a micro-flap).

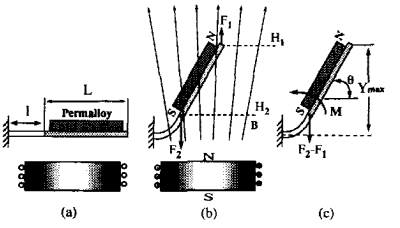

Fig. 3 Magnetic actuation of a flap by an external electromagnet. (a) Rest position when $H_{ext} = 0$; (b) out-of-plane actuation when $H_{ext} \neq 0$; F_1 and F_2 are the induced magnetic forces on the upper and lower edges of the plate; (c) a simplified analytical model of the flap; the effective bending moment, M, is $F_1 L cos\theta$.

$$\begin{aligned} F_1 &= M_s(WT)H_1, \\ F_2 &= M_s(WT)H_2, \end{aligned} \tag{3}$$

and M_s is the permalloy saturation magnetization, H_1 and H_2 are the magnetic field strengths near the top and bottom ends of the plate ($H_2 > H_1$). Since the I of the plate ($\propto (T+t)^3$) is much greater than that of the beams ($\propto t^3$), we consider the plate as a rigid body and concentrate on solving the beam bending. First, F_1 is translated to the free end of the beams, thereby simplifying the driving forces to a counter-clockwise torque $M = F_1(L\cos\theta)$ and a down-ward point force $F = F_2 - F_1$ (Fig. 3c). In our case, M bending is dominant and the beams deflect out-of-plane.

Ideally, to obtain the beam-end angular and vertical deflections, a non-linear differential equation under combined M and F should be solved [12]. For simplicity, however, we solve the angular/vertical deflections due to M and F separately and super-impose the results. This method is admissible here mostly because the force deflection predicted by the linear model is small (e.g. maximum angular deflection $< 10°$); also it is known that the actual deflection

will be even smaller than linear-model based calculations . In addition, the deflection by F will be approximately $8-10$ times smaller compared with the one caused by M. In all, we believe our method will provide a sound estimation of the over-all bending.

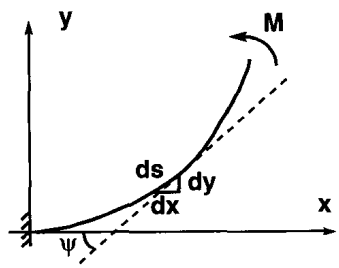

Fig. 4 Non-linear M bending.

To solve the torque deflection using the large deflection model, we start with the general relationship between a curvature and a torque (Fig. 4) at an arc length of s,

$$M = EI\frac{d\psi}{ds}, \tag{4}$$

where ψ is the slope at an arc length of s from (0,0). Under a constant M, the cantilever beam assumes the shape of an arc, with the radius of curvature being R ($R = EI/M$). The maximum angular deflection at the free end is

$$\psi_{max} = \theta_{torque} = k^2 l, \tag{5}$$

where $k^2 = M/EI$. The x and y coordinates at $s = l$ equal to

$$x(l) = \frac{1}{k^2}\sin(k^2 l) \tag{6}$$

$$y(l) = \frac{1}{k^2} - \frac{1}{k^2}\cos(k^2 l). \tag{7}$$

Note that when k^2 is small, $y(l)$ and $x(l)$ will be identical to what the small-deflection model predicts. The force bending can be solved by assuming F is applied at the free end of a pre-curved (circular-shaped) beam, in which case the maximum angular and vertical deflections are [11]

$$\theta_{force} = \frac{(\pi/2-1)FR^2}{EI}, \tag{8}$$

$$y_{force} = \frac{(3\pi/4-2)FR^2}{EI}. \tag{9}$$

The over-all angular deflection of the plate is then (Eq. 5 and 8)

$$\theta = \theta_{torque} - \theta_{force}, \tag{10}$$

and the maximum vertical deflection at the end of the plate equals to (Eq. 6, 9 and 10)

$$Y_{max} = y(l) - y_{force} + L \times \sin\theta. \tag{11}$$

Fracture Limit

The beams may be fractured when the maximum longitudinal strain at its fixed end exceeds that of the beam material (0.93%, [13]). The maximum strain can be estimated as follows,

$$\varepsilon_{max} \sim \frac{Mt}{EI} \leq 0.93\% = \frac{\theta_{frac}}{l}t. \tag{12}$$

In theory, θ_{frac} is the maximum angular beam deflection before fracture takes place.

DESIGN

The design of the micro-flaps has several facets, including mechanics (deflection and fracture strength), fluid dynamics(e.g. flow loading) and magnetism (magnetic force). A compromise among all four requirements must be sought, under the current flow and magnetic field parameters. Table 1 summarizes geometric parameters for two types of micro-flaps. Type-1 structures were actually assembled and wind-tunnel tested; Type-2 structures, on the other hand, were used mainly for device characterization in still air.

TYPE	L=W	T	l	w	t	δ_{max}(μm)	θ_{frac} (deg)
1	2	0.005	0.4	0.15	0.0018	8.2	118
2	1	0.005	0.4	0.1	0.0018	1.9	118

Table 1 Geometric parameters, gravitational deflection and maximum bending angle for two types of micro-flaps.

From Eq. 12, it is predicted that both flaps can be bent by a θ_{frac} of 118° before fracture occurs. This implies that these flaps will never reach their fracture point in a uniform magnetic field with field lines perpendicular to the chip substrate. However, it is worth noting that once inside a flow field, flow-induced bending and vibration can create θ larger than θ_{frac}.

The maximum flow loading on a fully deflected θ = 90°Type-1 flap is $210\mu N$ (Eq. 1) at a wind-tunnel flow speed of 19 m/s. This load will create a bending moment of approximately $210\ \mu N \times 1mm =$ 210 nNm. For a Type-2 flap under equal condition, the flow loading and bending moment are $53\mu N$ and 26 nNm, respectively.

FABRICATION

Fig. 5 illustrates major fabrication steps. Standard surface-micromachining procedures are followed to make polysilicon plate/beam structures on top of a 3 μm -thick phosphosilicate glass (PSG) sacrificial layer. The polysilicon is then covered by another 0.5 μm -thick PSG layer, which serves as a complimentary phosphorous doping source. During a 1

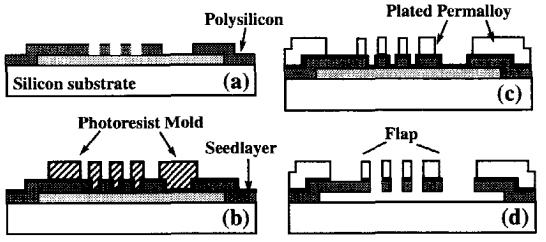

Fig. 5 Major fabrication steps of the micro-flaps. (a) Polysilicon plate and beam structure is deposited and patterned over the sacrificial material; (b) seed layer is evaporated and thick photoresist electroplating mold is made; (c) permalloy is electroplated and photoresist/seed-layer removed; (d) flaps are free-released by HF.

hour, 1050 °C stress-relief annealing, the polysilicon is doped from both sides to avoid intrinsic bending due to unbalanced doping concentration. The top PSG layer is later on removed by buffered hydrofluoric acid (BHF).

A 200 Å Cr and a 1800 Å Cu thin film are then evaporated over the polysilicon as the conductive seed layer for electroplating. A 5 μm -thick photoresist is applied and patterned to form molding frames, inside which permalloy ($Ni_{80}Fe_{20}$) electroplating takes place. This frame-plating technique was originally developed in the thin-film magnetic-head industry and is known to create high quality permalloy films [14, 15]. During the plating process, the wafer is affixed to the cathode and is oriented in such a way that the external magnetic field is parallel to the supporting beams. Electroplating takes place at 5 μm /hour under a bias-current density of 8 mA/cm^2. The resulting permalloy has a saturated magnetization of 1.35 Tesla, a relative permeability of 4500, a small remnant magnetization between 1 and 10 Gauss and a coercive force of 4 Oe [16].

After electroplating, the wafer is flood exposed with UV and the frame photoresist is removed. The seed layer is etched away by using Cu etchant and standard Cr mask etchant [17]. Flaps are then released by 50 % HF in 20 minutes. All permalloy plates stand well in HF, as well as in Cu and Cr etchant. To facilitate the sacrificial release process, etch holes (30 μm by 30 μm in size, and 250 μm apart) have been opened on the plate.

Since the micro-flaps have large surface areas and the supporting beams are soft(spring constant $\sim$ 100 μN / 1 mm=0.1 N/m), they can be easily pulled down by the surface tension to the substrate and form permanent bonds [18,19] if conventional drying techniques are used. To ensure high yield, we have developed a unique rinse/drying process to guarantee that almost 100 % yield is routinely achievable without using any complicated equipment for pressure and temperature cycling.

Shown in Fig. 6 are fabricated Type-2 flaps; no intrinsic bending was found for both types of flaps. Sequential video images of a micro-flap before and after the magnetic activation are in Fig. 7.

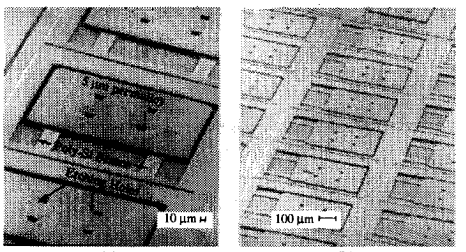

Fig. 6 SEM micrographs of fabricated Type-2 microactuators. The area of the plates is $1 \times 1 mm^2$. (a) A single flap; (b) a 2-D flap array.

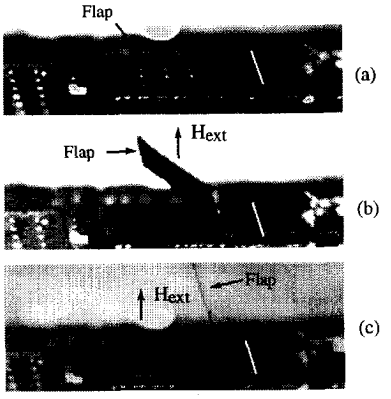

Fig. 7 Sequential snapshots of the flap actuation (a) before applying the magnetic field; (b) when $H_{ext} = 3.34 \times 10^4 A/m$ (B_{ext} = 420 Gauss); (c) when $H_{ext} = 6.4 \times 10^4 A/m$ (B_{ext}= 800 Gauss).

MAGNETIC ACTUATION

For testing the characteristics of individual Type-2 flaps in the still air, a strong industrial electromagnet is used. Actuation is observed by using a microscope-monitoring system (Fig. 8). The magnetic field calibration with respect to the vertical height is shown in Fig. 9: the field strength around the flaps is linear and can be expressed as $H = 21.5 \times 10^4 - 3.13 \times 10^4$ d(in mm), where d is the distance from the measurement point to the surface of the magnetic core. The angular and vertical deflection of the Type-1 actuator is directly measured from the monitor screen, with magnetic field of up to $6.4 \times 10^4 A/m$ at the chip surface. Fig. 10 shows the measured deflections, together with theoretical predictions using Eqs. 10 and 11. A good match between the bending theory and experimental θ and h is observed.

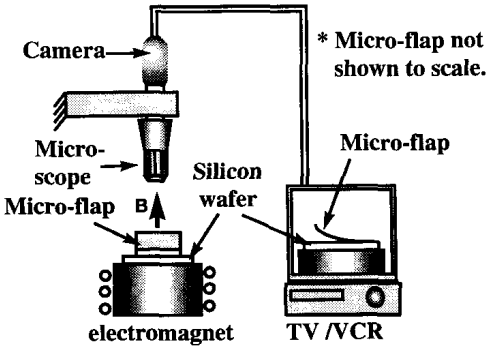

Fig. 8 A microscope/video flap monitoring system.

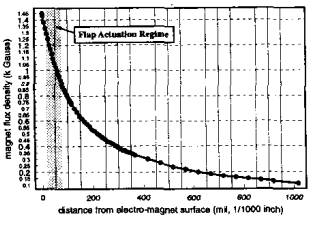

Fig. 9 Measured external magnetic field flux density vs. distance from the magnetic core.

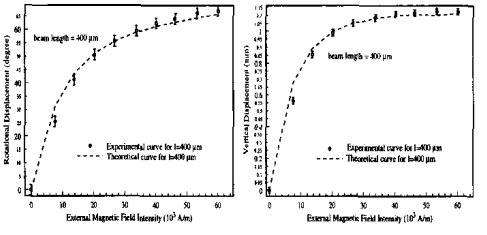

Fig. 10 Theoretical and experimental rotation angle θ and maximum vertical deflection y_{max} (as defined in Fig. 3c) vs. applied magnetic field intensity for a Type-2 flap. The plate size is 1×1 mm^2, beam length and width are 400 and 2×100 μm and the beam thickness is1.8 μm .

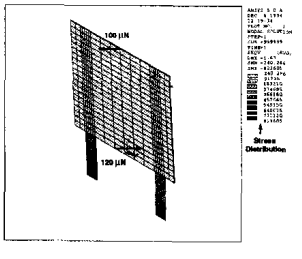

Fig. 11 An ANSYS © finite element analysis model.

A large-deflection finite element analysis (FEA) model of the flaps is also built (Fig. 11) and is currently used as a first-order verification of our analytical calculations. As an example, applying $F_1 = 100\mu$ N and $F_2 = 120\mu$ N on a Type-2 flap, Y_{ma}, θ, and ε_{max} are found to agree with results of Eq. 10, 11 and 12 to within 15 %.

DELTA-WING ASSEMBLY

The delta-wing model is made of aluminum; it has a span of 38 cm, and a top angle of 67° (Fig. 12a). Two grooves, parallel to the leading edges, are opened on the backside of the delta-wing (Fig. 12b). Each groove is approximately 250 $mm \times 4mm$ in size, 5 mm away from the leading edge; it holds three groups with a total of 54 electromagnets. As shown in Fig. 6, two linear arrays of $\sim$ 100 Type-1 micro-flaps are mounted on top of the electromagnets, flush with the delta-wing surface. To avoid magnet overheating, a maximum current of 1 A has been applied to the buried electromagnets to produce a maximum $H_{ext} = 2.1 \times 10^4$ A/m on the actuator plane (500 μm away from the magnet surface).

WIND TUNNEL TESTS

The delta-wing is then mounted on a 6-component force balance that records rolling moments and forces in three axis (Fig. 12). Initially, time-averaged measurement of the rolling moment (M_{roll}) was taken with the flaps kept on for at least four minutes. The resulting M_{roll} at different wind-tunnel flow speed is normalized with respect to the vortex lift moment, M_{vl}. Here, M_{vl} is the product of the vortex-lift force on one of the leading edges multiplied by the distance between the point-of-action and the delta-wing's central axis. A maximum M_{roll}/M_{vl} of 6.5 % at a flow speed of 19 m/s was observed. However, by then the

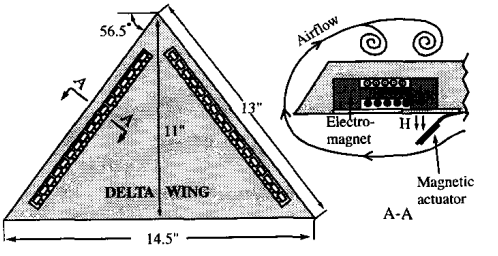

Fig. 12 Schematic of a delta-wing with two linear arrays of magnetic actuators flush-mounted close to the leading edges. (a) Plane view of a delta-wing with actuators installed; (b) cross-sectional view of the actuator/electromagnet on the delta-wing.

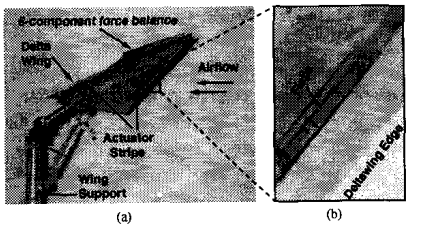

Fig. 13 A delta-wing under testing in a wind-tunnel. (a) the delta-wing is mounted on a 6-component force balance; (b) a close-up view of actuated flaps in a flow field.

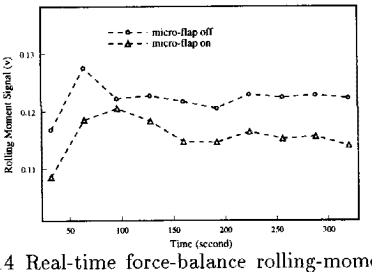

Fig. 14 Real-time force-balance rolling-moment output.

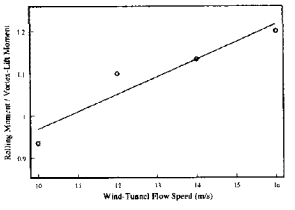

Fig. 15 M_r/M_{vl} generated by the actuation of one linear actuator array as a function of the average wind speed. $H_{ext} = 2.1 \times 10^4 A/m$; flow speed is 16 m/s.

force balance was not properly calibrated and long-term drift of the rolling moment (M_{roll})signal was later found. To ensure that the measured M_{roll} is indeed generated by the flap action and is not an artifact of signal drift, we then monitor the real-time M_{roll} changes by turning on and off one actuator array at approximately 1 Hz (Fig. 14). Very repeatable data of the M_{roll}/M_{vl} at various flow speed are obtained (Fig. 15); the maximum is 1.2 % at flow speed of 16 m/s.

The force balance has been calibrated and the drift problem solved. We experimentally studied the spatial optimization for more effective M_{roll} generation. Due to the limited supply of micro actuators, a rigid 250 mm long aluminum foil, extending 1–2 mm out of plane, (so called a passive flap) is used in this test. Except for its superior rigidity, this passive flap will simulate the effects of actuator micro flap arrays. First of all, a repeatable $\sim$ 1% M_{roll}/M_{vl} has been observed when the passive flap is at where the micro-flaps were originally located. We found that as the flap is positioned closer to the leading edge, the local flow speed is higher and the boundary layer is thinner, and more significant rolling moment can be created. In one test, as much as 10% time-averaged M_{roll}/M_{vl} is achieved (flow speed=16 m/s) when the passive flap is right on the leading edge. If the same percentage controlling capability is applied to a delta-wing F-15 fighter, a M_{roll} of 4×10^4 N-m could be generated, enough to turn the fighter 360 ° in $\sim$ 1 second. It is also expected that as the flow speed is increases, the rolling moment could become more significant.

We also find that operating the existing micro-flaps directly on the leading edge is impractical because the fluid loading is larger than before and it prevents the flaps from going out-of-plane. Second-generation flaps are currently being designed and fabricated; the new flaps will be more flexible yet more robust, and allows for even-stronger permalloy/magnetic field interaction.

CONCLUSIONS

Surface micromachined out-of-plane permalloy actuator arrays have been developed for controlling the rolling moment of a tail-less delta-wing. The actuator consists of a millimeter sized electroplated permalloy plate with supporting polysilicon beams and is driven by an external magnetic field. Large angular deflections (over 60 °) and vertical deflections (on the order of 1–2 mm) have been demonstrated. The magnetic forces and flow loading involved in the flap operation is on the order of hundred's of μN. Linear arrays of such flaps are positioned near the leading edges of the a delta-wing; wind-tunnel tests confirm that a rolling moment on the wing can be generated by the flap actuation.

ACKNOWLEDGEMENT

This work is supported by ARPA.

REFERENCES

1. W. Gu, O. Robinson, D. Rockwell, AIAA Journal, Vol. 31, No. 7, pp. 1177-1186, 1993.
2. K. Rinoie, Aeronautical Journal, Vol. 97 (961), pp. 33-38, 1993.
3. I.J. Busch-Vishniac, Sensors and Actuators, A 33, pp. 207-220, 1992.
4. C.H. Ahn and M.G. Allen, IEEE J. Micro Electro Mechanical Systems, Vol. 2(1), pp. 15–22, 1993.
5. H. Guckel, T.R. Christenson, K.J. Skrobis, T.S. Jung, J. Klein, K.V. Hartojo and I. Widjaja, 1993 IEEE Workshop on Micro Electro Mechanical-Systems, pp. 7–11, 1993.
6. B. Wagner, W. Benecke, G. Engelmann and J. Simon, Sensors and Actuators, A(32), pp. 598–603, 1992.
7. C. Liu, T. Tsao, Y.C. Tai and C.M. Ho, 1994 IEEE Workshop on Micro-Electro-Mechanical-Systems, pp. 57–62, 1994.
8. J.W. Judy, R.S. Muller and H.H. Zappe, 1994 IEEE Solid-State Sensor and Actuator Workshop, Hilton Head Island, SC, USA, pp. 43–48, 1994.
9. S.W. Yuan, Foundations of Fluid Mechanics, Prentice Hall, 1972.
10. CRC Handbook of Tables for Applied Engineering Science, the Chemical Rubber Co., 1970.
11. W.C. Young, Roark's Formulas for Stress and Strain, 6th Ed., McGraw-Hill, 1989.
12. R. Frisch-Fay, Flexible Bars, Butterworth, 1962.
13. Y.C. Tai, R. S. Muller, Technical Digest, IEEE Solid-State Sensors and Actuators Workshop, Hilton Head Island, SC, USA, pp. 88-91, 1988.
14. E.E. Castellani, J.V. Powers, L.T. Romankiw, U.S. Patent 4,102,756, 1978.
15. N.C. Anderson, C.R. Grove Jr., U.S. Patent 4,279,707, 1981.
16. W. Tang, V. Temesvary, S. Wu, Y.C. Tai and D.K. Miu, submitted to IEEE J. of MEMS.
17. Cr mask etchant, Transene Co., USA.
18. H. Guckel, J.J. Sniegowaki, T.R. Christenson, Sensors and Actuators, Vol. 20, pp. 117-122, 1989.
19. R.L. Alley, G.J. Cuan, R.T. Howe, K. Komvopoulos, Proceedings, IEEE Solid-State sensor and Actuator Workshop, Hilton Head, SC, USA, pp. 202-207, 1992.